Chinese Journal of Natural Medicines

Talaketides AG, linear polyketides with prostate cancer cytotoxic activity from the mangrove sediment-derived fungus *Talaromyces* sp. SCSIO 41027

Chunmei CHEN, Xueni WANG, Wenxuan FANG, Jiaqi LIANG, Jian CAI, Dehua YANG, Xiaowei LUO, Chenghai GAO, Xiangxi YI, Yonghong LIU, Xuefeng ZHOU

Citation: Chunmei CHEN, Xueni WANG, Wenxuan FANG, Jiaqi LIANG, Jian CAI, Dehua YANG, Xiaowei LUO, Chenghai GAO, Xiangxi YI, Yonghong LIU, Xuefeng ZHOU, Talaketides AG, linear polyketides with prostate cancer cytotoxic activity from the mangrove sediment-derived fungus *Talaromyces* sp. SCSIO 41027, Chinese Journal of Natural Medicines, 2024, 22(11), 1-10. doi: 10.1016/S1875-5364(24)60659-X.

View online: https://doi.org/10.1016/S1875-5364(24)60659-X

Available online at www.sciencedirect.com
ScienceDirect
Chinese Journal of Natural Medicines 2024, **22**(11): 1047-1056
doi: 10.1016/S1875-5364(24)60659-X
Chinese Journal of Natural Medicines

•Original article•

Talaketides A−G, linear polyketides with prostate cancer cytotoxic activity from the mangrove sediment-derived fungus *Talaromyces* sp. SCSIO 41027

CHEN Chunmei[1Δ], WANG Xueni[2Δ], FANG Wenxuan[2, 3], LIANG Jiaqi[1], CAI Jian[1], YANG Dehua[4], LUO Xiaowei[3], GAO Chenghai[3], YI Xiangxi[3], LIU Yonghong[1, 3*], ZHOU Xuefeng[1*]

[1] *CAS Key Laboratory of Tropical Marine Bio-Resources and Ecology, Guangdong Key Laboratory of Marine Materia Medica, South China Sea Institute of Oceanology, Chinese Academy of Sciences, Guangzhou 510301, China;*
[2] *Guangxi Zhuang Yao Medicine Center of Engineering and Technology, Guangxi University of Chinese Medicine, Nanning 530200, China;*
[3] *Guangxi Key Laboratory of Marine Drugs, Institute of Marine Drugs, Guangxi University of Chinese Medicine, Nanning 530200, China;*
[4] *The National Center for Drug Screening, Shanghai Institute of Materia Medica, Chinese Academy of Sciences, Shanghai 201203, China*

Available online 20 Nov., 2024

[ABSTRACT] Seven novel linear polyketides, talaketides A−G (**1**−**7**), were isolated from the rice media cultures of the mangrove sediment-derived fungus *Talaromyces* sp. SCSIO 41027. Among these, talaketides A−E (**1**−**5**) represented unprecedented unsaturated linear polyketides with an epoxy ring structure. The structures, including absolute configurations of these compounds, were elucidated through detailed analyses of nuclear magnetic resonance (NMR) and high-resolution mass spectrometry (HR-MS) data, as well as electronic custom distributors (ECD) calculations. In the cytotoxicity screening against prostate cancer cell lines, talaketide E (**5**) demonstrated a dose-dependent inhibitory effect on prostate cancer PC-3 cell lines, with an IC_{50} value of 14.44 μmol·L^{-1}. Moreover, compound **5** significantly inhibited the cloning formation of PC-3 cell lines and arrested the cell cycle in S-phase, ultimately inducing apoptosis. These findings indicate that compound **5** may serve as a promising lead compound for the development of a potential treatment for prostate cancer.

[KEY WORDS] Mangrove sediment-derived fungus; *Talaromyces* sp.; Linear polyketides; Cytotoxicity; Prostate cancer.
[CLC Number] R917 **[Document code]** A **[Article ID]** 2095-6975(2024)11-1047-10

Introduction

Marine natural products have been established as a significant source of lead compounds [1, 2]. Fungi derived from mangrove sediments represent a rich reservoir of structurally diverse and bioactive metabolites with unique chemical structures [3]. The genus *Talaromyces* (Eurotiomycetes, Trichocomaceae), established approximately 70 years ago to classify the teleomorphs of certain *Penicillium* species [4], has been found to occur in diverse environments, both terrestrial and marine [5, 6]. Various structural classes have been identified in *Talaromyces* spp. [5, 6], including alkaloids [7], terpenoids [8], polyketides [9], and steroids [10]. These compounds have demonstrated interesting and potent activities, such as antimicrobial [11, 12], anticancer [12], anti-inflammatory [8-10], and enzyme inhibitory properties [13]. Consequently, *Talaromyces* has recently garnered significant attention from biologists, chemists, and pharmacologists.

Prostate cancer represents a significant health concern, ranking as the second most frequently diagnosed cancer among men and a leading cause of cancer-related mortality [14]. While patients with localized prostate cancer generally experience favorable outcomes following standard treatment proto-

[Received on] 10-Feb.-2024
[Research funding] This work was supported by the Key-Area Research and Development Program of Guangdong Province (No. 2023B1111050008), the National Natural Science Foundation of China (Nos. U23A20528, U20A20101), Guangdong Local Innovation Team Program (No. 2019BT02Y262), and the Postdoctoral Fellowship Program of CPSF (No. GZC20232777).
[*Corresponding author] E-mails:yonghongliu@scsio.ac.cn (LIU Yonghong); xfzhou@scsio.ac.cn (ZHOU Xuefeng)
[Δ]These authors contributed equally to this work.
These authors have no conflict of interest to declare.

cols [15], those with locally advanced or extensive metastatic disease often develop resistance to castration therapy, ultimately succumbing to disease progression [16]. Recent decades have witnessed substantial advancements in the understanding of prostate cancer genetics and underlying molecular mechanisms, facilitating the development of novel therapeutic agents targeting metastatic castration-resistant prostate cancer [15]. However, persistent challenges such as low cure rates and drug resistance underscore the critical need for identifying more efficacious therapeutic interventions for prostate cancer management.

In recent years, our research group has identified several marine natural products, including 5'-epiequisetin [17], stemphone C [18], malaymycin [19], and DC1149B [20], as promising lead compounds for anti-prostate cancer. In continuation of this work, we have directed our current investigation towards discovering novel metabolites from marine fungi, specifically focusing on the secondary metabolites of the mangrove sediment-derived fungus *Talaromyces* sp. SCSIO 41027. This study reports the isolation, structural elucidation, and cytotoxic evaluations of seven new linear polyketides, designated as talaketides A−G (**1**−**7**).

Results and Discussion

The fungal strain *Talaromyces* sp. SCSIO 41027 was isolated from a mangrove sediment sample (21.235° N, 110.451° E) in the South China Sea. The strain was cultivated on a rice solid medium and subsequently extracted with ethyl acetate. The resulting extract underwent fractionation and purification through iterative chromatography techniques, including silica gel, ODS, and semi-preparative C_{18} high-performance liquid chromatography (HPLC) chromatography, yielding talaketides A−G (**1**−**7**) (Fig. 1) .

Talaketide A (**1**) was isolated as a colorless oil. The molecular formula was determined to be $C_{16}H_{20}O_5$ with 7 degrees of unsaturation based on high-resolution electrospray ionization mass spectrometry (HR-ESI-MS) data (*m*/*z* 293.1396 $[M + H]^+$, Calcd. for $C_{16}H_{21}O_5$, 293.1384). IR absorptions at 1714 cm^{-1} indicated the presence of carbonyl groups. The 1D nuclear magnetic resonance (NMR) data (Table 1) and het-

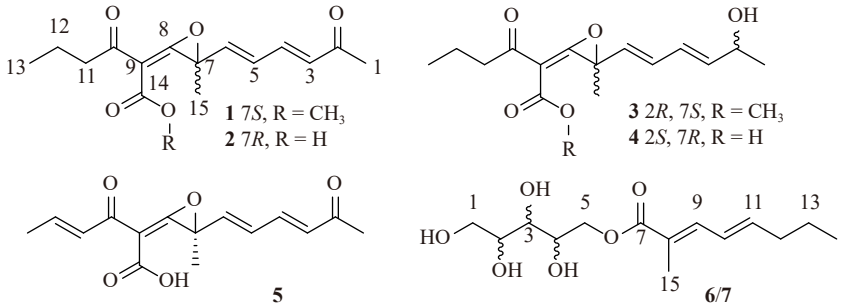

Fig. 1 Structures of polyketides from *Talaromyces* sp. SCSIO 41027.

Table 1 The ^{1}H (500 MHz) and ^{13}C (125 MHz) NMR data of compounds 1−4 in DMSO-d_6.

No.	1		2		3		4	
	δ_C type	δ_H (*J* in Hz)	δ_C type	δ_H (*J* in Hz)	δ_C type	δ_H (*J* in Hz)	δ_C type	δ_H (*J* in Hz)
1	27.0, CH_3	2.22 (s)	27.0, CH_3	2.22 (s)	23.5, CH_3	1.11 (d, 6.5)	23.6, CH_3	1.11 (d, 6.5)
2	198.2, C		198.1, C		66.0, CH	4.16 (p, 6.0)	66.0, CH	4.16 (p, 5.5)
3	132.5, CH	6.23 (d, 15.5)	132.4, CH	6.23 (d, 16.0)	142.1, CH	5.85 (dd, 15.0, 5.5)	142.0, CH	5.84 (dd, 15.0, 5.5)
4	141.6, CH	6.50 (dd, 15.5, 11.0)	141.7, CH	7.23 (dd, 16.0, 10.5)	126.0, CH	6.13 (dd, 15.0, 10.5)	126.1, CH	6.13 (dd, 15.0, 10.5)
5	129.2, CH	7.23 (dd, 16.0, 10.5)	129.1, CH	6.49 (dd, 15.5, 11.0)	131.2, CH	6.27 (dd, 15.5, 10.5)	131.0, CH	6.26 (dd, 15.5, 10.5)
6	137.1, CH	6.26 (d, 15.5)	137.4, CH	6.26 (d, 15.5)	127.2, CH	5.64 (d, 15.5)	127.4, CH	5.63 (d, 15.5)
7	90.3, C		90.0, C		90.5, C		90.2, C	
8	196.1, C		196.9, C		197.0, C		197.7, C	
9	105.6, C		106.2, C		105.5, C		106.1, C	
10	198.5, C		198.3, C		198.2, C		197.8, C	
11	32.0, CH_2	3.01 (m)	32.0, CH_2	3.01 (m)	32.0, CH_2	2.99 (m)	31.9, CH_2	2.98 (m)
12	19.3, CH_2	1.72 (qd, 7.5, 1.0)	19.4, CH_2	1.72 (q, 7.5)	19.3, CH_2	1.70 (q, 7.5)	19.4, CH_2	1.70 (q, 7.5)
13	13.5, CH_3	0.97 (t, 7.5)	13.5, CH_3	0.96 (t, 7.5)	13.5, CH_3	0.95 (t, 7.5)	13.5, CH_3	0.95 (t, 7.5)
14	162.2, C		163.1, C		162.4, C		163.2, C	
15	21.4, CH_3	1.51 (s)	21.5, CH_3	1.50 (s)	21.4, CH_3	1.46 (s)	21.4, CH_3	1.45 (s)
16	51.2, CH_3	3.70 (s)			51.1, CH_3	3.71 (s)		

eronuclear single quantum coherence (HSQC) experiment of **1** revealed three carbonyl carbons (δ_C 198.5, 198.2, 162.2), two olefinic (one oxygenated) carbons (δ_C 196.1, 105.6), one oxygenated quaternary carbon (δ_C 90.3), four olefinic methylenes ($\delta_{H/C}$ 6.50/141.6, 6.26/137.1, 6.23/132.5, 7.23/129.2), two methylenes ($\delta_{H/C}$ 3.01/32.0, 1.72/19.3), and four methyls ($\delta_{H/C}$ 3.70/51.2, 2.22/27.0, 1.51/21.4, 0.97/13.5). The ^{1}H-^{1}H correlation spectroscopy (COSY) spectrum (Fig. 2) of **1** indicated two isolated spin systems H-3/H-4/H-5/H-6 and H_2-11/H_2-12/H_3-13. The heteronuclear multiple bond correlation (HMBC) spectrum (Fig. 2) showed correlations from H_3-1 to C-2 and C-3, from H-3 to C-2 and C-5, from H-5 and H-6 to C-7, from H_3-16 to C-6, C-7, and C-8, and from H_2-11 to C-9, C-10, and C-12, suggesting the presence of a linear chain from C-1 to C-13. The chemical shift of CH_3-16 ($\delta_{H/C}$ 3.70/51.2) and the HMBC from H_3-16 to C-14 indicated that CH_3-16 was an oxygenated methyl attached to the oxygen atom of the ester group. The chemical shifts of C-7 and C-8, the remaining oxygen atom, and one degree of unsaturation suggested that C-7 and C-8 form an epoxy ring. Consequently, the structure of **1** was elucidated as a linear polyketide and named talaketide A.

The coupling constants $J_{H\text{-}3/H\text{-}4,\ H\text{-}5/H\text{-}6}$ (15.5 Hz) of the double bond in **1** confirmed that the configurations of Δ^3 and Δ^5 were *E*. Furthermore, the absolute configuration of the chiral atom C-7 was elucidated through electronic custom distributors (ECD) calculations. The experimental ECD spectrum of **1** exhibited excellent correlation with the calculated ECD spectrum of (7*S*)-**2** (Fig. 3), demonstrating a distinct negative Cotton effect at 260 nm. Consequently, the stereochemistry of compound **1** was established as 7*S*.

Talaketide B (**2**) was isolated as a colorless oil. The molecular formula was determined to be $C_{15}H_{18}O_5$ (seven degrees of unsaturation), with one -CH_2 less than **1**. The ^{1}H and ^{13}C NMR spectroscopic data (Table 1) of **2** closely resembled those of **1**, with the notable absence of a methoxy signal in **2**, suggesting the presence of a carboxyl group instead of a methyl ester group at C-14. This hypothesis was corroborated by the molecular formula and the 2D NMR data (Fig. 2), thus confirming the planar structure of compound **2**. The coupling constants $J_{H\text{-}3/H\text{-}4,\ H\text{-}5/H\text{-}6}$ (15.0 and 15.5 Hz) indicated that the configurations of double bonds Δ^3 and Δ^5 were *E*. Furthermore, a comparison of the experimental ECD spectrum of **2** with the calculated ECD spectrum of (7*R*)-**2** showed excellent agreement, displaying a positive Cotton effect at 260 nm (Fig. 3), thereby establishing the absolute configuration of **2** as 7*R*.

The 1D NMR data and a molecular formula of talaketides C and D (**3** and **4**) indicated a structural similarity to compound **1**, with one less degree of unsaturation. A detailed analysis of the NMR spectra (Table 1) of **3** revealed that the carbonyl carbon signal ($\delta_{H/C}$ 198.2, C-2) in **1** was replaced by an oxygenated methylene signal ($\delta_{H/C}$ 4.16/66.0, CH-2) in **3**. The HMBCs (Fig. 2) from H_3-1 and H-3 to C-2, the ^{1}H-^{1}H COSY signals between H_3-1/H-2/H-3/H-4/H-5/H-6, and the changed chemical shifts of CH-3 and CH-4 further confirmed the presence of a hydroxy group at CH-2 in **3** instead of a carbonyl group. Similarly, compound **4**, which exhibited the molecular formula $C_{15}H_{20}O_5$ based on the HR-ESI-MS data, was an analog of **3**, featuring a carboxyl group at C-14 instead of a methyl ester group, as supported by the 2D NMR data (Fig. 2).

The substantial coupling constants of the double bonds Δ^3 and Δ^5 in compounds **3** and **4** indicated an *E* configuration. The modified Mosher's method [21] was employed to esterify the hydroxyl group at C-2 of compounds **3** and **4**, with a successful reaction only for compound **3**. Compound **3** was treated with (*R*)- and (*S*)-MPA, respectively, yielding (*R*)- and (*S*)-MPA esters. These esters were then analyzed using ^{1}H-NMR spectroscopy, and the $\Delta\delta_{RS}$ values (δ_R-δ_S) were used to assign the 2*R* configuration to compound **3** (Fig. 4). Following the bulkiness rule [22, 23], $Rh_2(OCOCF_3)_4$ complexes of **3** and **4** were generated in $CDCl_3$. The negative and positive signs of the Cotton effect for the E band at 355 nm in the ECD spectrum (Fig. 3) indicated 2*R* and 2*S* configurations of **3** and **4**, respectively. Subsequent ECD calculations confirmed the absolute configurations at C-7 of **3** and **4** as 7*S* and 7*R*, respectively (Fig. 3).

Talaketide E (**5**) exhibited a molecular formula of $C_{15}H_{16}O_5$, as determined by HR-ESI-MS data (*m*/*z* 277.1028, $[M + H]^+$, Calcd. for 277.1071), indicating eight degrees of unsaturation (one more than **2**). Analysis of the NMR data (Table 2) revealed structural similarities to **2**, with the addition of two olefinic methylene signals ($\delta_{H/C}$ 7.25/146.5,

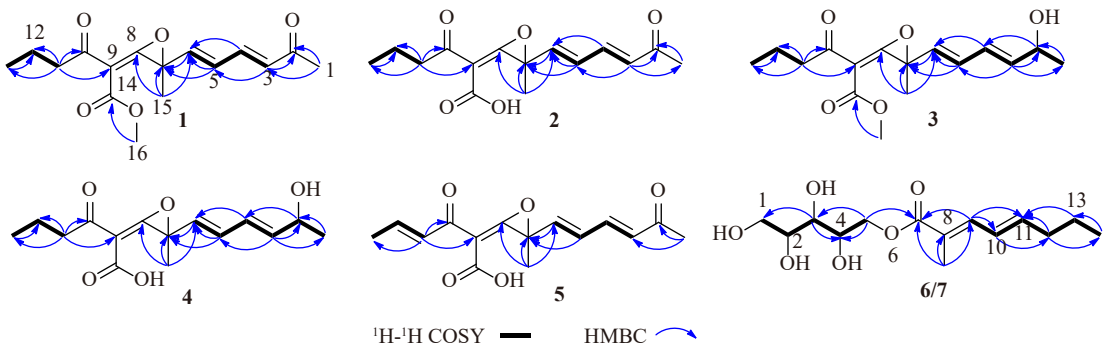

Fig. 2 Key ^{1}H-^{1}H COSY correlations and HMBCs of compounds 1−7.

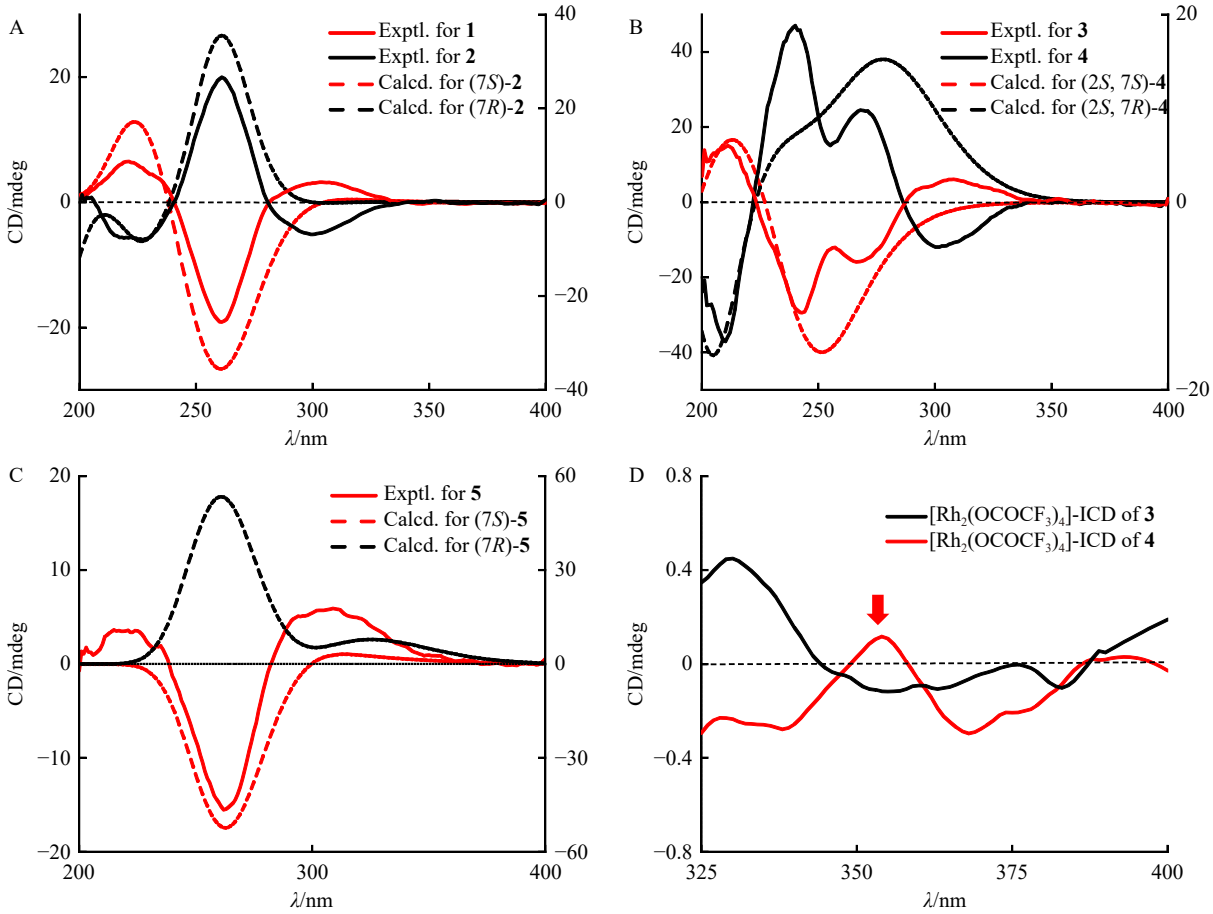

Fig. 3 Experimental and calculated ECD spectra of compounds 1−5 (A, B, C) and ICD curves of 3 and 4 induced by $Rh_2(OCOCF_3)_4$ in $CDCl_3$ (D).

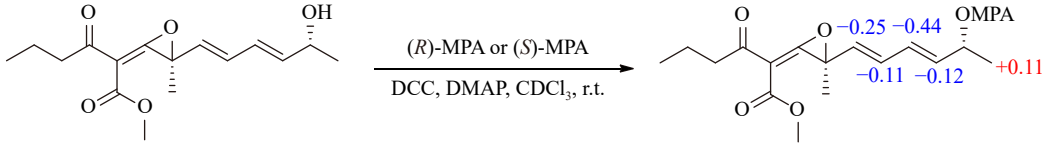

Fig. 4 $\Delta\delta_{RS}$ (δ_R-δ_S) data for the MPA esters of 3.

7.21/119.7) and the absence of two methine signals. The formation of a double bond Δ^{11} in **5**, replacing the saturated single bond in **2**, was confirmed by ^{1}H-^{1}H COSY signals (Fig. 2) between H-11/H-12/H_3-13 and HMBCs (Fig. 2) from H-11 to C-9, C-10, and C-13. The large coupling constants of the double bonds Δ^3, Δ^5, and Δ^{11} indicated their *E* configuration. Furthermore, the stereochemistry of **5** was determined to be 7*S* based on the perfect match between the experimental ECD spectrum and the calculated ECD spectrum of (7*S*)-**5** (Fig. 3). Consequently, compound **5** was assigned as (7*S*)-talaketide E.

Talaketides F and G (**6** and **7**) shared the same molecular formula of $C_{14}H_{24}O_6$, with three degrees of unsaturation. The 1D NMR data for **6** (Table 2) revealed signals of one ester carbon (δ_C 167.8), one sp^2 quaternary carbon (δ_C 124.7), three olefinic methines ($\delta_{H/C}$ 6.15/143.0, 7.16/138.3, 6.43/126.2), three oxygenated sp^3 quaternary carbons ($\delta_{H/C}$ 3.39/70.2, 3.71/69.7, 3.74/68.5), four methylene groups ($\delta_{H/C}$ 3.39/62.8, 4.03, 4.30/67.2, 2.16/34.6, 1.43/21.6) (two oxygenated), and two methyl groups ($\delta_{H/C}$ 0.89/13.6, 1.87/12.5). The ^{1}H-^{1}H COSY spectrum indicated two isolated spin systems H-9/H-10/H-11/H_2-12/H_2-13/H_3-14 and H_2-1/H-2/H-3/H-4/H_2-5 (Fig. 2). The linkage of the two spin systems was deduced from key HMBCs (Fig. 2) from H-9 to C-7, from H_2-5 to C-7, and from H_3-15 to C-7, C-8, and C-9, which further revealed that the methyl (CH_3-15) was attached to C-8. Upon examination of the 1D and 2D NMR data for **7**, it exhibited a planar structure consistent with that of **6**. The large coupling constant of $J_{H\text{-}10/H\text{-}11}$ (14.5 Hz) indicated that the double bond Δ^{10} was in the *E* configuration. The small carbon chemical shift of CH_3-15 (δ_C 12.5) suggested that Δ^8 was also in the *E* configuration (γ-pyrone effect) [24, 25]. Significant differences were observed in the carbon and hydrogen chemical shifts of CH_2-1, CH-2, CH-3, CH-4, and CH_2-5. Based on coupling constants and compound shifts, it was proposed that they

were the C-2 and C-4 diastereomers. However, determining the absolute configurations of C-2, C-3, and C-4 proved challenging due to their hydroxyl groups and flexible structure.

Two human prostate cancer cell lines, PC-3 (androgen receptor negative) and 22Rv1 (androgen receptor positive), were utilized in the antiproliferative assay for compounds **1**−**7** (Fig. 5A). Compound **5**, identified as the most potent, exhibited a dose-dependent inhibition of cell viability in the prostate cancer cell line PC-3 and the normal prostate stromal cell line WPMY-1, as determined by MTT assay (Fig. 5). The IC_{50} values were 14.44 ± 0.34 and 18.20 ± 0.44 μmol·L^{-1}, respectively. The positive control, docetaxel, demonstrated inhibitory effects with IC_{50} values of 0.12 and 0.51 μmol·L^{-1}, respectively. The selectivity cytotoxicity index (SI) of compound **5** was calculated as 1.26. Furthermore, the presence of the double bond Δ^{11} in **5** may contribute to its enhanced cytotoxic activity against prostate cancer cells.

To further evaluate the impact of **5** on PC-3 cell proliferation, we performed a plate clone formation assay. The results demonstrated that **5** significantly inhibited the clone formation of PC-3 cells in a dose-dependent manner (Fig. 6). Notably, the PC-3 cell line is a prostate cancer cell line that lacks androgen receptor expression. These findings suggest that compound **5** exerts its anti-prostate cancer effects not through modulation of the androgen receptor signaling pathway but *via* alternative mechanisms.

To further elucidate the mechanism of cytotoxicity induced by compound **5**, we investigated its effect on PC-3 cell apoptosis using flow cytometry (Fig. 7). The results demonstrated that compound 5 triggered cell apoptosis in a dose-

Table 2 The ^{1}H (500 MHz) and ^{13}C (125 MHz) NMR data of compounds 5−7 in DMSO-d_6.

No.	5		6		7	
	δ_C type	δ_H (*J* in Hz)	δ_C type	δ_H (*J* in Hz)	δ_C type	δ_H (*J* in Hz)
1	27.0, CH_3	2.21 (s)	62.8, CH_2	3.39 (overlapped)	63.5, CH_2	3.60 (dd, 11.0, 3.5) 3.41 (dd, 11.0, 6.0)
2	198.2, C		70.2, CH	3.39 (overlapped)	71.0, CH	3.49 (ddd, 9.0, 6.0, 3.5)
3	132.4, CH	6.25 (d, 16.0)	69.7, CH	3.71 (dd, 6.5, 2.0)	70.7, CH	3.28 (dd, 8.5, 2.0)
4	141.6, CH	7.25 (overlapped)	68.5, CH	3.74 (td, 6.5, 3.5)	67.4, CH	3.94 (ddd, 7.5, 5.5, 2.0)
5	129.0, CH	6.52 (dd, 15.5, 11.0)	67.2, CH_2	4.30 (dd, 11.0, 2.5) 4.03 (dd, 11.0, 6.5)	66.1, CH_2	4.10 (dd, 11.0, 7.5) 4.04 (dd, 11.0, 5.5)
6	137.7, CH	6.29 (d, 15.0)	167.8, C		167.6, C	
7	89.7, C		124.7, C		124.6, C	
8	196.0, C		138.3, CH	7.16 (d, 11.5)	138.4, CH	7.13 (d, 11.0)
9	102.9, C		126.2, CH	6.43 (dd, 14.5, 11.5)	126.1, CH	6.43 (dd, 14.5, 11.5)
10	184.5, C		143.0, CH	6.15 (dt, 14.5, 7.0)	143.2, CH	6.16 (dt, 14.5, 7.0)
11	119.7, CH	7.21 (d, 16.0)	34.6, CH_2	2.16 (q, 7.0)	34.6, CH_2	2.16 (q, 7.0)
12	146.5, CH	7.25 (overlapped)	21.6, CH_2	1.43 (h, 7.5)	21.6, CH_2	1.42 (h, 7.5)
13	19.3, CH_3	2.05 (d, 6.0)	13.6, CH_3	0.89 (t, 7.5)	13.6, CH_3	0.89 (t, 7.5)
14	162.3, C		12.5, CH_3	1.87 (s)	12.5, CH_3	1.87 (s)
15	21.6, CH_3	1.53 (s)	21.4, CH_3	1.51 (s)	21.5, CH_3	1.50 (s)
16			51.2, CH_3	3.70 (s)		

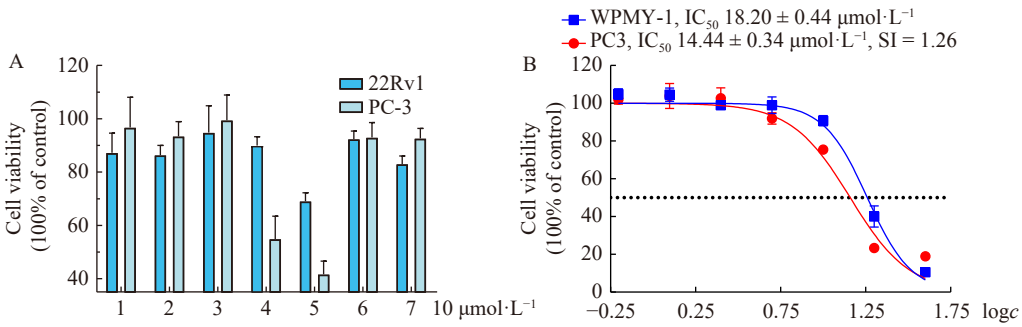

Fig. 5 Cytotoxicity against prostate cancer cells. (A) Cytotoxicity of compounds 1−7 against prostate cancer cell lines PC-3 and 22Rv1. (B) Compound 5 exhibited varying degrees of inhibition on prostate cancer cell viability.

dependent manner, with docetaxel serving as a positive control.

To elucidate the mechanism underlying prostate cancer cell proliferation inhibition, we analyzed the cell cycle distribution of PC-3 cells. As illustrated in Fig. 8, treatment with the M-phase blocker docetaxel resulted in a significant accumulation of PC-3 cells in the M-phase, leading to a substantial increase in the G_2/M ratio. Conversely, cells treated with compound **5** exhibited a marked increase in the percentage of S-phase cells, indicating that compound **5** arrested the cell cycle at S-phase, thereby impeding cell proliferation.

Enzymes phosphatidylinositol 3-kinase (PI3K) and 6-phosphofructo-2-kinase/fructose-2,6-biphosphatase 3 (PFK-2/FBPase3, PFKFB3), which play a crucial role in regulating glycolysis in cancer cells and their proliferation and survival [26], were utilized to assess the enzyme inhibitory activities of compounds **1**−**7**. The results indicated that only compound **4** exhibited moderate inhibitory activity against the PI3K protein, with an IC_{50} value of 37.73 μmol·L^{-1} (positive control, zstk, IC_{50} 45.43 nmol·L^{-1}). The PI3K/Akt pathway is a target for prostate cancer chemotherapy, regulating cell cycle progression, apoptosis, and neoplastic transformation [27, 28]. Based on these findings, it can be inferred that **5** exerted its effects on prostate cancer PC-3 cells through alternative pathways. Collectively, these results suggest that **5** represents a promising lead compound for prostate cancer pharmacotherapy.

Conclusions

In conclusion, seven novel polyketides, talaketides A−G

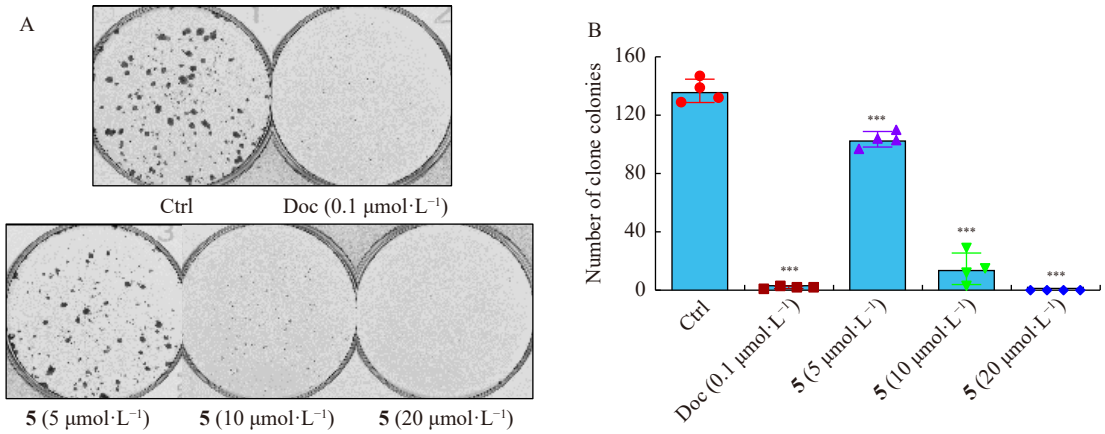

Fig. 6 Compound 5 reduced PC-3 cell colony formation in a dose-dependent manner (A, B).

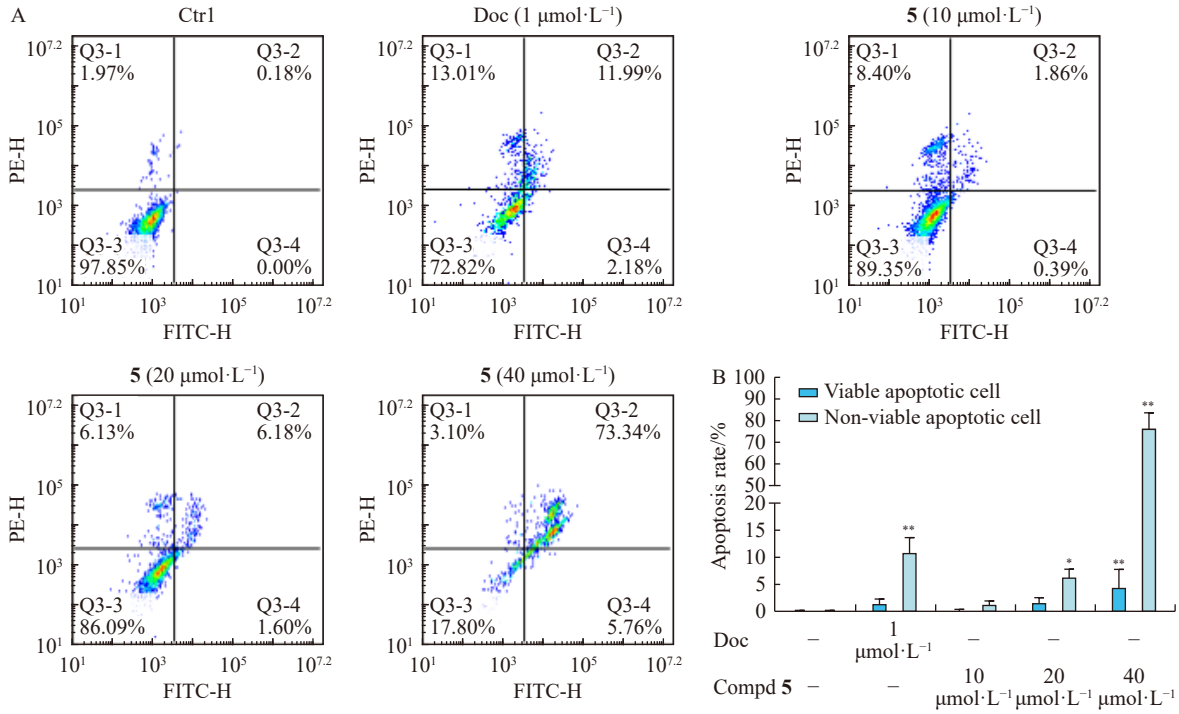

Fig. 7 Compound 5 induced apoptosis in PC-3 cells in a dose-dependent manner (A, B).

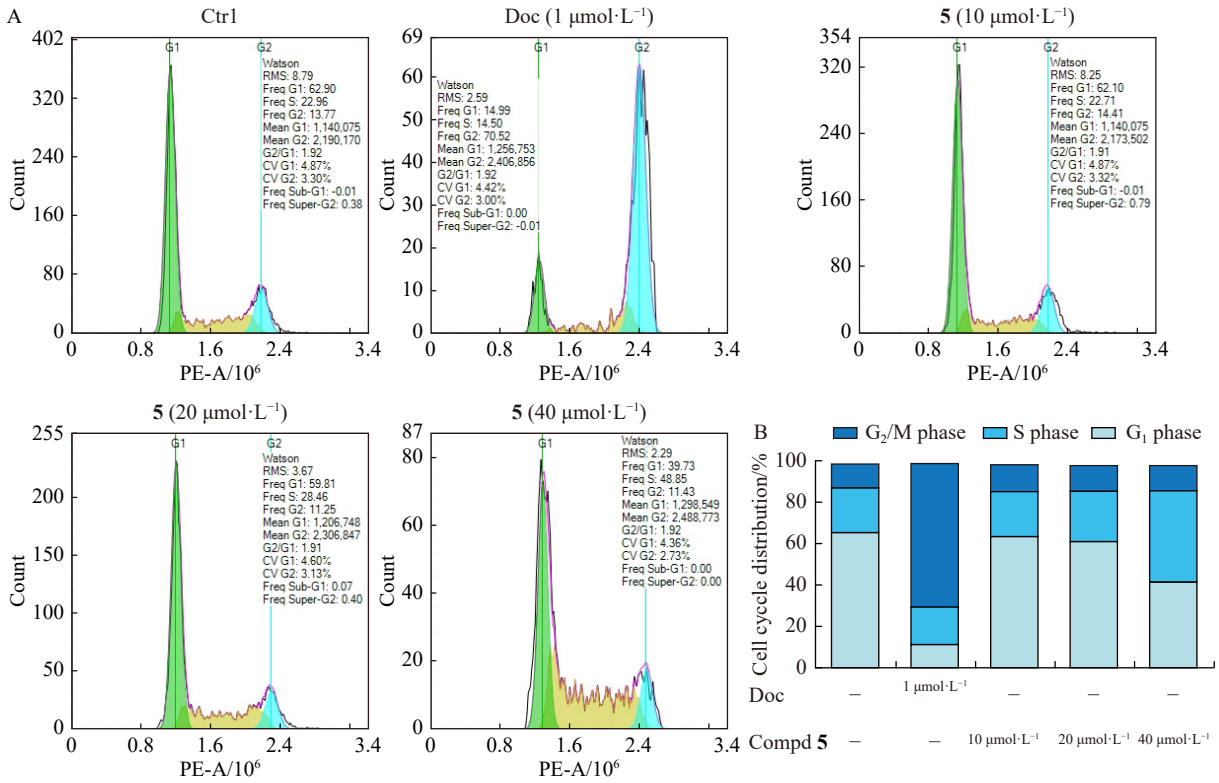

Fig. 8 Compound 5 induced PC-3 cell cycle arrest at S-phase (A, B).

(**1**−**7**), were isolated from the mangrove sediment-derived fungus *Talaromyces* sp. SCSIO 41027 and structurally characterized through comprehensive spectroscopic analyses and ECD calculations. Notably, compounds **1**−**5** represent unprecedented unsaturated linear polyketides featuring an epoxy ring structure. Talaketide E (**5**) exhibited a dose-dependent inhibitory effect on prostate cancer PC-3 cells, with an IC_{50} value of 14.44 μmol·L^{-1}. Furthermore, compound **5** significantly impaired the cloning ability of PC-3 cells and arrested the cell cycle in S-phase, ultimately inducing apoptosis. These findings underscore the importance of natural products as a valuable source of highly potent lead compounds and present these molecules as promising candidates for further structural optimization in prostate cancer models.

Experimental

General experimental procedures

The UV and IR spectra were obtained using a Shimadzu UV-2600 PC spectrometer (Shimadzu) and an IR Affinity-1 spectrometer (Shimadzu). Optical rotations were determined using an Anton Paar MPC 500 polarimeter. HR-ESI-MS spectra were recorded with a Bruker maXis Q-TOF mass spectrometer. NMR spectra were recorded on a Bruker Avance-500 and Avance III HD 700 MHz Digital NMR Spectrometer (Bruker BioSpin International AG, Switzerland) using tetramethylsilane as internal standard, with chemical shifts recorded as *δ*-values. Semipreparative HPLC was performed on the Hitachi Primaide with a DAD detector, using an ODS column (YMC-pack ODS-A, 10 mm × 250 mm, 5 μm). Thin-layer chromatography analysis (TLC) and column chromatography (CC) were conducted on plates precoated with silica gel GF_{254} (10−40 μm) and over silica gel (200−300 mesh) (Qingdao Marine Chemical Factory) and Sephadex LH-20 (Amersham Biosciences, Uppsala, Sweden), respectively. Spots were visualized on TLC (Qingdao Marine Chemical Factory) under 254 nm UV light. All solvents used were of analytical grade (Tianjin Fuyu Chemical and Industry Factory).

Reagents and antibodies

Docetaxel was obtained from Selleck Chemicals (Cat# RP56976). RPMI 1640 medium was acquired from Gibco (Cat# 8120018). Fetal bovine serum was procured from Gemini (Cat# 900-108). Charcoal-stripped fetal bovine serum (FBS) was purchased from Biological Industries (Cat# 04-201-1A). Thiazolyl blue tetrazolium bromide (Cat# M8180) and crystal violet stain solution (Cat# G1063) were obtained from Solarbio Life Sciences. The Human Apoptosis Array Kit was sourced from R&D Systems (Cat# ARY009). NuPAGETM 10% Bis-Tris Gel (Cat# NP0302BOX), eBioscience™ Annexin V-FITC apoptosis detection kit (Cat# BMS500FI-300), FxCycle™ PI/RNase staining solution (Cat# F10797) and Vybrant cell-labeling solutions (V22885) were acquired from Invitrogen. All antibodies utilized in this study were procured from Proteintech Group (CDK4, Cat# 66950-1-lg; CDK6, Cat# 66278-1-lg; Cyclin D1, Cat# 26939-1-AP; RB1, Cat# 10048-1-lg; E2F1, Cat# 66515-1-lg; Survivin, Cat# 66495-1-lg; p21, Cat# 10355-1-AP).

Fungal material

The strain SCSIO 41027 was isolated from the rhizosphere sediment of a mangrove forest collected in Zhanjiang, Guangdong Province, China (21.235° N, 110.451° E) in 2019. The strain was preserved on Müller Hinton broth (MB) agar (malt extract 15 g, sea salt 10 g, agar 16 g, H_2O 1 L, pH 7.4−7.8) slants at 4 °C and deposited at the Key Laboratory of Tropical Marine Bio-resources and Ecology, Chinese Academy of Sciences. The ITS1-5.8S-ITS4 sequence region (GenBank accession No. OR984205) of strain SCSIO 41027 was described in the Supporting Information and exhibited significant homology to the sequence of *Talaromyces oumae-annae* (accession No. OP797636.1). Consequently, it was classified as a *Talaromyces* sp. and designated as *Talaromyces* sp. SCSIO 41027.

Fermentation and extraction

The strain *Talaromyces* sp. SCSIO 41027 was cultured on MB agar plates at 28 °C for seven days. The seed medium (comprising 15 g malt extract and 30 g artificial sea salt in 1.0 L of tap distilled H_2O, pH 7.4−7.8) was inoculated with strain SCSIO 41027 and incubated at 28 °C for three days on a rotating shaker (180 r·min^{-1}). Large-scale fermentation of fungal SCSIO 41027 was conducted for 30 days at room temperature in 60 1 L conical flasks containing solid rice medium (each flask contained 150 g of rice, 5.4 g of artificial sea salt, and 180 mL of H_2O). The entire fermented culture was subsequently extracted with EtOAc three times, yielding a reddish-brown extract (210 g).

Isolation and purification

The organic extract underwent silica gel CC using step gradient elution with petroleum ether/CH_2Cl_2 (0%−100%, *V*/*V*) and CH_2Cl_2/CH_3OH (0%−100%, *V*/*V*) to yield fifteen subfractions (Frs. 1−15) based on TLC properties. Fifteen small fractions (Frs. 5-1−5-15) were obtained by ODS reversed-phase medium-pressure liquid chromatography (MPLC) separation [CH_3OH/H_2O (10%−100%)] of fraction Fr. 5. Fr.5-6 was separated and purified using semi-preparative HPLC [34% CH_3CN/H_2O (0.04% TFA), 2 mL·min^{-1}] to yield compound **4** (11.3 mg, t_R = 15.6 min) and a mixed fraction Fr. 5-6-2 (t_R = 20.2 min). Fr. 5-6-2 was further separated by HPLC [53% CH_3OH/H_2O (0.04% TFA), 2 mL·min^{-1}] to obtain compounds **2** (2.9 mg, t_R = 24.5 min) and **5** (5.4 mg, t_R = 30.0 min). Fr. 5-7 was isolated with semi-preparative HPLC [60% CH_3CN/H_2O (0.04% TFA), 2 mL·min^{-1}] to obtain compound **1** (5.1 mg, t_R = 11.5 min), and a mixed fraction Fr.5-7-1 (t_R = 8.0 min). Compound **3** (5.0 mg, t_R = 15.5 min) was further purified from Fr. 5-7-1 by semi-preparative HPLC [69% CH_3OH/H_2O (0.04% TFA), 2 mL·min^{-1}]. The fraction Fr.8 was separated by the ODS column gradient elution of the separated fraction [CH_3OH/H_2O (10%−100%)] to obtain eight small fractions (Frs. 8-1−8-10). Fr. 8-8 was separated by semi-preparative liquid phase [56% CH_3OH/H_2O (0.04% TFA), 2 mL·min^{-1}] to obtain compounds **6** (4.4 mg, t_R = 20.8 min) and **7** (5.8 mg, t_R = 22.8 min).

Talaketide A (***1***): colorless oil; $[\alpha]_D^{25}$ −80 (*c* 0.1, MeOH); UV (MeOH) λ_{max} (log ε) 200 (3.52), 227 (3.42), 265 (4.00) nm; ECD (0.30 mg·mL^{-1}, MeOH) λ_{max} ($\Delta\varepsilon$) 200 (+1.35), 221 (+8.72), 261 (−25.49), 303 (+4.27) nm; IR (film) ν_{max} 2964, 1714, 1670, 1585, 1436, 1394, 1253, 1197, 1126, 1045, 1001 cm^{-1}; ^{1}H and ^{13}C NMR data, Table 1; HR-ESI-MS *m/z* 293.1396 $[M + H]^+$ (Calcd. for $C_{16}H_{21}O_5$, 293.1384), 315.1213 $[M + Na]^+$ (Calcd. for $C_{16}H_{20}NaO_5$, 315.1203), 607.2532 $[2M + Na]^+$ (Calcd. for $C_{32}H_{40}NaO_{10}$, 607.2514).

Talaketide B (***2***): colorless oil; $[\alpha]_D^{25}$ +51 (*c* 0.1, MeOH); UV (MeOH) λ_{max} (log ε) 200 (4.01), 231 (4.35), 265 (3.95) nm; ECD (0.15 mg·mL^{-1}, MeOH) λ_{max} ($\Delta\varepsilon$) 200 (−9.55), 210 (−14.82), 240 (+18.81), 255 (+6.06), 268 (+9.82), 301 (−4.77) nm; IR (film) ν_{max} 2972, 2931, 1714, 1697, 1681, 1575, 1456, 1386, 1201, 1138, 1041, 1026, 993 cm^{-1}; ^{1}H and ^{13}C NMR data, Table 1; HR-ESI-MS *m/z* 281.1393 $[M + H]^+$ (Calcd. for $C_{15}H_{21}O_5$, 281.1384), 303.1206 $[M + Na]^+$ (Calcd. for $C_{15}H_{20}NaO_5$, 303.1203).

Talaketide C (***3***): colorless oil; $[\alpha]_D^{25}$ −14 (*c* 0.1, MeOH); UV (MeOH) λ_{max} (log ε) 200 (3.71), 228 (3.89), 265 (3.59) nm; ECD (0.30 mg·mL^{-1}, MeOH) λ_{max} ($\Delta\varepsilon$) 200 (+2.80), 211 (+6.02), 243 (−11.75), 257 (−4.82), 266 (−6.36), 308 (+2.45) nm; IR (film) ν_{max} 1716, 1577, 1456, 1386, 1201, 1126, 1045, 991 cm^{-1}; ^{1}H and ^{13}C NMR data, Table 1; HR-ESI-MS *m/z* 295.1538 $[M + H]^+$ (Calcd. for $C_{16}H_{23}O_5$, 295.1540), 317.1357 $[M + Na]^+$ (Calcd. for $C_{16}H_{22}NaO_5$, 317.1359), 611.2824 $[2M + Na]^+$ (Calcd. for $C_{32}H_{44}NaO_{10}$, 611.2827)

Talaketide D (***4***): colorless oil; $[\alpha]_D^{25}$ + 22 (*c* 0.1, MeOH); UV (MeOH) λ_{max} (log ε) 200 (3.85), 228 (3.72), 265 (4.14) nm; ECD (0.30 mg·mL^{-1}, MeOH) λ_{max} ($\Delta\varepsilon$) 200 (+0.15), 221 (−7.57), 261 (+26.61), 300 (−6.84) nm; IR (film) ν_{max} 1714, 1680, 1593, 1437, 1257, 1205, 1141, 1047, 1003 cm^{-1}; ^{1}H and ^{13}C NMR data, Table 1; HR-ESI-MS *m/z* 277.1089 $[M - H]^-$ (Calcd. for $C_{15}H_{17}O_5$, 277.1081).

Talaketide E (***5***): colorless oil; $[\alpha]_D^{25}$ −13 (*c* 0.1, MeOH) UV (MeOH) λ_{max} (log ε) 200 (4.09), 229 (3.92), 266 (4.23) nm; ECD (0.15 mg·mL^{-1}, MeOH) λ_{max} ($\Delta\varepsilon$) 200 (−0.71), 221 (+3.58), 262 (−15.55), 309 (+5.92) nm; IR (film) ν_{max} 1705, 1635, 1595, 1438, 1396, 1255, 1205, 1136, 1047, 999 cm^{-1}; ^{1}H and ^{13}C NMR data, Table 2; HR-ESI-MS *m/z* 277.1078 $[M + H]^+$ (Calcd. for $C_{15}H_{17}O_5$, 277.1071).

Talaketide F (***6***): colorless oil; $[\alpha]_D^{25}$ + 2 (*c* 0.1, MeOH) UV (MeOH) λ_{max} (log ε) 200 (3.63), 221 (3.48), 265 (4.01) nm; IR (film) ν_{max} 3375, 2960, 2922, 1697, 1683, 1653, 1589, 1456, 1261, 1242, 1097, 972 cm^{-1}; ^{1}H and ^{13}C NMR data, Table 2; HR-ESI-MS *m/z* 289.1642 $[M + H]^+$ (Calcd. for $C_{14}H_{25}O_6$, 289.1646), 311.1459 $[M + Na]^+$ (Calcd. for $C_{14}H_{24}NaO_6$, 311.1465).

Talaketide G (***7***): colorless oil; $[\alpha]_D^{25}$ −5 (*c* 0.1, MeOH) UV (MeOH) λ_{max} (log ε) 200 (3.50), 222 (3.33), 265 (3.99) nm; IR (film) ν_{max} 3288, 1705, 1681, 1456, 1205, 1138, 1099, 1068, 1035, 966 cm^{-1}; ^{1}H and ^{13}C NMR data, Table 2; HR-ESI-MS *m/z* 289.1648 $[M + H]^+$ (Calcd. for $C_{14}H_{25}O_6$, 289.1646), 311.1466 $[M + Na]^+$ (Calcd. for $C_{14}H_{24}NaO_6$,

311.1465).

Mosher's Method

Compound **3** (0.8 mg) was dissolved in $CDCl_3$ (600 μL), followed by the addition of (*R*)-MPA (1.4 mg) or (*S*)-MPA (1.2 mg), DCC (1.6 mg), and DMAP (1.0 mg). The mixture was stirred at room temperature for 10 h. The (*R*)-MPA ester (**3a**) was purified using Hitachi Primaide HPLC with an ODS C_{18} column (90% CH_3OH/H_2O containing 0.04% TFA, flow rate: 3 mL·min^{-1}), yielding **3a** (0.2 mg, t_R = 9.8 min). The (*S*)-MPA ester (**3b**) was purified using the same HPLC conditions, yielding **3a** (0.4 mg, t_R = 10.2 min). Compound **4** (2.0 mg) was prepared following the same protocol as for compound **3**.

(*R*)-MPA Ester (**3a**). ^{1}H NMR (700 MHz, DMSO-d_6) δ_H 6.18 (1H, dd, *J* = 15.5, 10.5 Hz, H-5), 5.75 (2H, overlapped, H-3/H-4), 5.46 (1H, d, *J* = 15.5 Hz, H-6), 1.26 (3H, d, *J* = 6.5 Hz, H_3-1).

(*S*)-MPA Ester (**3b**). ^{1}H NMR (700 MHz, DMSO-d_6) δ_H 6.29 (1H, dd, *J* = 15.5, 10.5 Hz, H-5), 6.19 (1H, dd, *J* = 15.5, 10.5 Hz, H-4), 5.87 (1H, dd, *J* = 15.5, 6.0 Hz, H-3), 5.71 (1H, d, *J* = 15.5 Hz, H-6), 1.15 (3H, d, *J* = 6.5 Hz, H_3-1).

$[Rh_2(OCOCF_3)_4]$-ICD measurement

The samples of compounds **3** and **4** (0.2 mg) were dissolved in 300 μL [$Rh_2(OCOCF_3)_4$] complex (0.6 mg·mL^{-1} in $CDCl_3$) and subjected to ECD measurements. The initial ECD spectrum was recorded immediately after mixing, and its time evolution was monitored until reaching a stationary state (15 min after mixing). The inherent ECD was subtracted. The observed signs of the E bands at 355 nm in the induced CD spectra were correlated with absolute configurations of the C-2 secondary alcohols in compounds **3** and **4**.

Computation section

The conformational analyses of the compounds were conducted using Spartan'14 and the Molecular Merck force field [29]. Conformers with a Boltzmann population exceeding 1% underwent further optimization using Gaussian 09 at the B3LYP/6-31G (d) level in methanol. The stable conformers were selected for ECD calculations at the optimized conformers were then selected for ECD calculations at the B3LYP/6-311G (d, p) level in methanol. The aggregate ECD data were weighted according to Boltzmann distribution, and the ECD curves and enantiomeric ECD curves were generated using GaussView 6.0 software with a half-bandwidth of 0.33 eV. The Boltzmann-calculated contributions of each conformer, following UV correction, were utilized for this purpose.

Cell culture

The 22Rv1, PC-3, and WPMY-1 cell lines were obtained from the National Collection of Authenticated Cell Cultures (Shanghai, China). The cell lines were authenticated by short tandem repeat (STR) profiling, and only cells within 15 passages were utilized in the experiments. 22Rv1 cells were cultured in RPMI 1640 medium supplemented with 10% (*V*/*V*) FBS, 100 U·mL^{-1} penicillin, and 100 μg·μL^{-1} streptomycin. PC-3 cells were maintained in DMEM F12 medium with identical additives. WPMY-1 cells were cultured in DMEM (Gibco, China) medium containing 5% (*V*/*V*) FBS (Biological Industries, Israel), 100 U·mL^{-1} penicillin, and 100 μg·μL^{-1} streptomycin.

MTT assay

Cell viability was assessed using the MTT assay as previously described [17]. Briefly, cells were seeded overnight in a 96-well plate at a density of 5 × 10^3 per well and subsequently treated with varying concentrations of compound **5** for the designated time period. Following exposure to compound **5** for a specific duration, MTT solution was added to the cell culture wells for 4 h. The OD_{570} values were then measured using a Hybrid Multi-Mode Reader (Synergy H1, BioTek). This experiment was conducted in triplicate. The IC_{50} values were calculated by using GraphPad 9.0 software. The SI was determined as the ratio of IC_{50} in normal cells to IC_{50} in tumor cells.

Plate clone formation assay

PC-3 cells were seeded in a 6-well plate at a density of 1000 cells per well and incubated overnight. The following day, they were treated with DMSO (0.1%, *V*/*V*), docetaxel (1), and compound **5** (5, 10, and 20 μmol·L^{-1}) for the required duration, respectively. The culture medium was replenished every 72 h until visible colony formation was observed after approximately 15 d. Cells were then fixed with 4% formaldehyde for 30 min, washed with PBS buffer to remove the fixative, and stained with crystal violet solution. After 30 min of staining, the stain solution was removed, and the cells were rinsed again with PBS buffer. Colonies were photographed using a colony counter (GelCount, Oxford Optronix). The experiment was conducted independently in triplicate.

Apoptosis and cell cycle assay

PC-3 cells were seeded in a 6-well plate at a density of 2.0 × 10^5 per well overnight. The cells were then treated with DMSO (0.1%, *V*/*V*), docetaxel (1 μmol·L^{-1}), and compound **5** (10, 20, and 40 μmol·L^{-1}), respectively, for 48 h. Subsequently, cells were harvested and stained according to the protocols of eBioscience™ Annexin V-FITC apoptosis detection kit and FxCycle™ PI/RNase staining solution. Cell apoptosis and cell cycle distribution were analyzed using flow cytometry (NovoCyte, Agilent). This experiment was conducted independently in triplicate.

Enzyme inhibitory assay [30]

The enzyme inhibitory activity of these compounds against PI3K [31] and PFKFB3 [26] was evaluated using previously reported methods. Initial screening was conducted using a compound concentration of 20 μmol·L^{-1}. Subsequently, a more detailed PI3K enzyme inhibitory activity assay was performed to determine the IC_{50} value of **4** at concentrations ranging from 0.625 to 80 (0.625, 1.25, 2.5, 5, 10, 20, 40, and 80 μmol·L^{-1}).

Statistical analysis

All analyses were performed using GraphPad Prism 9 (GraphPad Software, United States). Results were expressed as mean ± standard deviation (SD) and subjected to one-way

ANOVA. Inter-group comparisons were conducted using Dunnett's *t*-test. Statistical significance was established at $^{*}P < 0.05$, $^{**}P < 0.01$, and $^{***}P < 0.001$.

Supplementary data

Supplementary data to this article can be requested by sending E-mails to the corresponding author.

References

[1] Carroll AR, Copp BR, Davis RA, *et al*. Marine natural products [J]. *Nat Prod Rep*, 2023, **40**: 275-325.

[2] Newman DJ, Cragg GM. Natural products as sources of new drugs over the nearly four decades from 01/1981 to 09/2019 [J]. *J Nat Prod*, 2020, **83**: 770-803.

[3] Li K, Chen S, Pang X, *et al*. Natural products from mangrove sediments-derived microbes: structural diversity, bioactivities, biosynthesis, and total synthesis [J]. *Eur J Med Chem*, 2022, **230**: 114117.

[4] Benjamin CR. Ascocarps of *Aspergillus* and *Penicillium*. [J]. *Mycologia*, 1955, **47**: 669-687.

[5] Nicoletti R, Bellavita R, Falanga A. The outstanding chemodiversity of marine-derived *Talaromyces* [J]. *Biomolecules*, 2023, **13**: 1021.

[6] Zhai MM, Li J, Jiang CX, *et al*. The bioactive secondary metabolites from *Talaromyces* species [J]. *Nat Prod Bioprospect*, 2016, **6**: 1-24.

[7] Chen S, He L, Chen D, *et al*. Talaramide A, an unusual alkaloid from the mangrove endophytic fungus *Talaromyces* sp. (HZ-YX1) as an inhibitor of mycobacterial PknG [J]. *New J Chem*, 2017, **41**: 4273-4276.

[8] Chen C, Sun W, Liu X, *et al*. Anti-inflammatory spiroaxane and drimane sesquiterpenoids from *Talaromyces minioluteus* (*Penicillium minioluteum*) [J]. *Bioorg Chem*, 2019, **91**: 103166.

[9] Cai J, Zhou XM, Yang X, *et al*. Three new bioactive natural products from the fungus *Talaromyces assiutensis* JTY2 [J]. *Bioorg Chem*, 2020, **94**: 103362.

[10] Zhang M, Li Q, Li S, *et al*. An unprecedented ergostane with a 6/6/5 tricyclic 13(14→8)abeo-8, 14-seco skeleton from *Talaromyces adpressus* [J]. *Bioorg Chem*, 2022, **127**: 105943.

[11] Zang Y, Genta-Jouve G, Escargueil AE, *et al*. Antimicrobial oligophenalenone dimers from the soil fungus *Talaromyces stipitatus* [J]. *J Nat Prod*, 2016, **79**: 2991-2996.

[12] Anand BG, Thomas CK, Prakash S. *In vitro* cytotoxicity and antimicrobial activity of *Talaromyces flavus* SP5 inhabited in the marine sediment of Southern Coast of India [J]. *Chin J Nat Med*, 2016, **14**: 913-921.

[13] Ren J, Ding SS, Zhu A, *et al*. Bioactive azaphilone derivatives from the fungus *Talaromyces aculeatus* [J]. *J Nat Prod*, 2017, **80**: 2199-2203.

[14] Siegel RL, Miller KD, Fuchs HE, *et al*. Cancer statistics, 2022 [J]. *CA Cancer J Clin*, 2022, **72**: 7-33.

[15] Attard G, Parker C, Eeles RA, *et al*. Prostate cancer [J]. *Lancet*, 2016, **387**: 70-82.

[16] Nelson WG, De Marzo AM, Isaacs WB. Mechanisms of disease: Prostate cancer [J]. *N Engl J Med*, 2003, **349**: 366-381.

[17] Wang X, Luo X, Gan X, *et al*. Analysis of regulating activities of 5'-epiequisetin on proliferation, apoptosis, and migration of prostate cancer cells *in vitro* and *in vivo* [J]. *Front Pharmacol*, 2022, **13**: 920554.

[18] Cai J, Wang X, Gan X, *et al*. New chlorinated metabolites and antiproliferative polyketone from the mangrove sediments-derived fungus *Mollisia* sp. SCSIO41409 [J]. *Mar Drugs*, 2022, **21**: 32.

[19] Xie Y, Guo L, Huang J, *et al*. Cyclopentenone-containing tetrahydroquinoline and geldanamycin alkaloids from *Streptomyces malaysiensis* as potential anti-androgens against prostate cancer cells [J]. *J Nat Prod*, 2021, **84**: 2004-2011.

[20] Cai J, Wang X, Yang Z, *et al*. Thiodiketopiperazines and alkane derivatives produced by the mangrove sediment-derived fungus *Penicillium ludwigii* SCSIO 41408 [J]. *Front Microbiol*, 2022, **13**: 857041.

[21] Seco JM, Quiñoá E, Riguera R. The assignment of absolute configuration by NMR [J]. *Chem Rev*, 2004, **104**: 17-117.

[22] Cai J, Gao L, Wang Y, *et al*. Discovery of a novel anti-osteoporotic agent from marine fungus-derived structurally diverse sirenins [J]. *Eur J Med Chem*, 2024, **265**: 116068.

[23] Bai J, Liu D, Yu S, *et al*. Amicoumacins from the marine-derived bacterium *Bacillus* sp. with the inhibition of NO production [J]. *Tetrahedron Lett*, 2014, **55**: 6286-6291.

[24] Peng B, Cai J, Xiao Z, *et al*. Bioactive polyketides and benzene derivatives from two mangrove sediment-derived fungi in the Beibu Gulf [J]. *Mar Drugs*, 2023, **21**: 327.

[25] Suzuki S, Horii F, Kurosu H. Theoretical investigations of the γ-gauche effect on the ^{13}C chemical shifts produced by oxygen atoms at the γ position by quantum chemistry calculations [J]. *J Mol Struct*, 2009, **919**: 290-294.

[26] Boyd S, Brookfield JL, Critchlow SE, *et al*. Structure-based design of potent and selective inhibitors of the metabolic kinase PFKFB3 [J]. *J Med Chem*, 2015, **58**: 3611-3625.

[27] Chang F, Lee JT, Navolanic PM, *et al*. Involvement of PI3K/Akt pathway in cell cycle progression, apoptosis, and neoplastic transformation: a target for cancer chemotherapy [J]. *Leukemia*, 2003, **17**: 590-603.

[28] Hamidi A, Song J, Thakur N, *et al*. TGF-b promotes PI3K-AKT signaling and prostate cancer cell migration through the TRAF6-mediated ubiquitylation of p85a [J]. *Sci Signal*, 2017, **10**: eaal4186.

[29] Chen C, Xiao L, Luo X, *et al*. Identifying marine-derived tanzawaic acid derivatives as novel inhibitors against osteoclastogenesis and osteoporosis *via* downregulation of NF-κB and NFATc1 activation [J]. *J Med Chem*, 2024, **67**: 2602-2618.

[30] Ye Y, Liang J, She J, *et al*. Two new alkaloids and a new butenolide derivative from the Beibu Gulf sponge-derived fungus *Penicillium* sp. SCSIO 41413 [J]. *Mar Drugs*, 2022, **21**: 27.

[31] Tian C, Yang C, Wu T, *et al*. Discovery of cinnoline derivatives as potent PI3K inhibitors with antiproliferative activity [J]. *Bioorg Med Chem Lett*, 2021, **48**: 128271.

Cite this article as: CHEN Chunmei, WANG Xueni, FANG Wenxuan, *et al*. Talaketides A−G, linear polyketides with prostate cancer cytotoxic activity from the mangrove sediment-derived fungus *Talaromyces* sp. SCSIO 41027 [J]. *Chin J Nat Med*, 2024, **22**(11): 1047-1056.